Solar Energy Materials & Solar Cells 159 (2017) 167–171

Contents lists available at ScienceDirect

Solar Energy Materials & Solar Cells

journal homepage: www.elsevier.com/locate/solmat

Spectral hemispherical reflectivity of nonstoichiometric cerium dioxide

Simon Ackermann, Aldo Steinfeld *

Department of Mechanical and Process Engineering, ETH Zürich, Sonneggstrasse 3, 8092 Zürich, Switzerland

A R T I C L E I N F O

Article history:
Received 23 August 2016
Accepted 31 August 2016
Available online 19 September 2016

Keywords:
Ceria
Nonstoichiometry
Reflectivity
Spectroscopy
Solar radiation

A B S T R A C T

Nonstoichiometric ceria, $CeO_{2-\delta}$, has emerged as a promising redox material for thermochemically splitting H_2O and CO_2 using concentrated solar energy. Knowledge of its radiative properties is crucial for the design of efficient solar reactors. Samples of various nonstoichiometries ($0 \le \delta \le 0.0377$) were prepared by thermal reduction in a thermogravimetric analyzer at high temperatures ($T \ge 1473$ K) and under low oxygen partial pressures ($p_{O2} \le 2.5 \cdot 10^{-4}$ atm). The spectral hemispherical reflectivity was measured using a spectroscopic goniometry system in the spectral range 300–2800 nm. A porous ceria sample with interconnected μm-sized pores showed comparable selectivity because of its high optical thickness. The total hemispherical reflectivity was computed for emission temperatures in the range 900–6000 K relevant to solar reactors.

1. Introduction

Using concentrated solar radiation, thermochemical redox cycles based on nonstoichiometric metal oxides are capable of splitting H_2O and CO_2 to produce H_2 and CO (syngas), the precursor for the synthesis of conventional transportation liquid fuels [1]. Ceria (CeO_2) is currently considered the state-of-the-art redox material due to its favorable thermodynamics, rapid kinetics, and morphological stability over a wide range of temperatures [2–14]. The two-step thermochemical cycle based on nonstoichiometric ceria is represented by:

Reduction at T_{red}:

$$\frac{1}{\delta_{red}-\delta_{ox}}CeO_{2-\delta_{ox}} \rightarrow \frac{1}{\delta_{red}-\delta_{ox}}CeO_{2-\delta_{red}} + \frac{1}{2}O_2 \tag{1}$$

Oxidation at T_{ox}:

$$\frac{1}{\delta_{red}-\delta_{ox}}CeO_{2-\delta_{red}} + H_2O \rightarrow \frac{1}{\delta_{red}-\delta_{ox}}CeO_{2-\delta_{ox}} + H_2 \tag{2a}$$

$$\frac{1}{\delta_{red}-\delta_{ox}}CeO_{2-\delta_{red}} + CO_2 \rightarrow \frac{1}{\delta_{red}-\delta_{ox}}CeO_{2-\delta_{ox}} + CO \tag{2b}$$

where δ_{ox} and δ_{red} are the oxygen nonstoichiometries before and after reduction, respectively. In the first step, Eq. (1), ceria is endothermally reduced in an atmosphere of low oxygen partial pressure, p_{O2}, and at elevated temperatures, typically $T_{red} > 1573$ K, with process heat delivered by concentrated solar radiation. In the second step, Eq. (2), the reduced ceria is exothermally re-oxidized with H_2O and/or CO_2 to generate H_2 and/or CO at lower temperatures, typically $T_{ox} < 1573$ K. δ_{red} and δ_{ox} strongly depend on T_{red}, T_{ox}, and p_{O2}. The difference $\delta_{red}-\delta_{ox}$ determines the maximum molar amount of fuel capable of being produced per cycle and per mole of ceria.

The design and optimization of solar chemical reactors for effecting the redox cycle demands the development of numerical heat transfer models using accurate radiative properties because radiation is the dominant heat transport phenomena at T_{red} [15,16]. Specifically for reticulated porous ceria structures, the accurate determination of the absorbed and scattered portion of radiation requires the knowledge of the hemispherical reflectivity of ceria r_{CeO_2} as a function of wavelength λ and nonstoichiometry δ:

$$\alpha(\lambda, \delta) = \left(1 - r_{CeO_2}(\lambda, \delta)\right)\cdot\beta \tag{3}$$

$$\sigma(\lambda, \delta) = r_{CeO_2}(\lambda, \delta)\cdot\beta \tag{4}$$

where α is the absorption coefficient, σ the scattering coefficient, and β the effective extinction coefficient. On the other hand, β depends solely on the morphology and can be determined by applying pore-level Monte Carlo ray tracing on the exact 3D digital representation of the porous structures obtained by computed tomography [17]. To date however, there isn't any data reporting the spectral reflectivity of ceria as a function of its nonstoichiometry and measurement data on the optical properties of ceria are scarce. Hass et al. [18] investigated the refractive index and the absorption coefficient of evaporated CeO_2 films in the wavelength range 0.22–

* Corresponding author.
E-mail address: aldo.steinfeld@ethz.ch (A. Steinfeld).

http://dx.doi.org/10.1016/j.solmat.2016.08.036

Nomenclature

c_1	speed of light [m s^{-1}]
h_p	Planck constant [J s]
k_B	Boltzmann constant [J K^{-1}]
L_{CeO_2}	detector signal for the ceria sample [V]
L_{ref}	detector signal for the reference sample [V]
$r_{CeO_2,\lambda}$	spectral hemispherical reflectivity of ceria [–]
R_{CeO_2}	total hemispherical reflectivity of ceria [–]
$r_{ref,\lambda}$	spectral hemispherical reflectivity of the reference sample [–]
T	temperature [K]

Greek symbols

α	absorption coefficient [m^{-1}]
β	extinction coefficient [m^{-1}]
δ	nonstoichiometry [–]
λ	wavelength [nm]
σ	scattering coefficient [m^{-1}]

Acronym

TGA	thermogravimetric analyzer

1.0 μm. Touloukian et al. [19] reported normal spectral reflectivity of CeO_2 of electron beam deposited films and of sintered powder. Fangxin et al. [20] and Marabelli et al. [21] measured the UV–visible reflectivity of nanocrystalline ceria and studied the absorption characteristics by Kramers-Kronig transformation. Ganesan et al. [22] determined the albedo and the scattering coefficient of stoichiometric CeO_2 by measuring the directional-hemispherical reflectance in the range of 0.35–2.0 μm.

In this work, the spectral hemispherical reflectivity of sintered polycrystalline ceria was measured for a wide range of λ and δ relevant for the solar redox cycle. An empirical correlation is least-squares fitted to the total hemispherical reflectivity as a function of δ and the blackbody radiation temperature. Additionally, the reflectivity of a porous ceria sample with ~0.26 porosity and a mean pore diameter of ~10 μm [23] is measured to investigate the effect of the μm-sized pores.

2. Methodology

2.1. Optical setup

Measurements were performed with a goniometry spectroscopic system [24,25], shown schematically in Fig. 1. It consists of: 1) Xe-arc lamp as light source that emits radiation in the range 170–3000 nm and approximates a blackbody at 6200 K in the visible range; 2) aspherical Czerny-Turner type double monochromator; 3) mechanical beam chopper to modulate at a frequency of 417 Hz for minimizing background noise; 4) imaging lens; 5) iris to adjust the ray cone angle; 6) mechanical slit; 7) integrating sphere; 8) sample holder; 9) photodetector; 10) lock-in amplifier, and 11) data acquisition system.

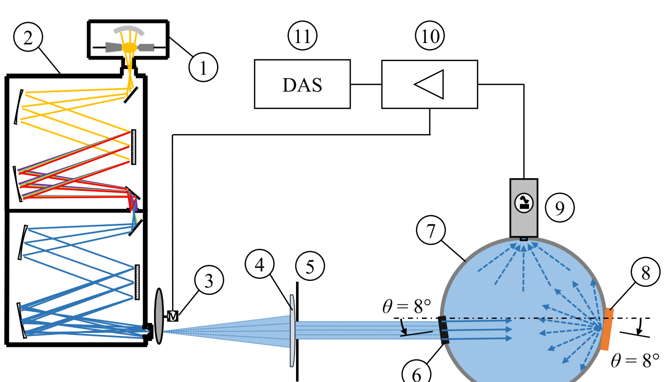

Fig. 1. Schematic of the spectroscopic system that consists of a: 1) xenon-arc lamp, 2) double monochromator, 3) chopper, 4) imaging lens, 5) iris, 6) mechanical slit, 7) integrating sphere, 8) sample holder, 9) photodetector, 10) lock-in amplifier, 11) data acquisition system.

Each measurement is performed with a ceria sample and a reference (calibrated) sample. The spectral hemispherical reflectivity of the ceria sample, $r_{CeO_2,\lambda}$, is then calculated by:

$$\frac{L_{CeO_2}}{L_{ref}} = \frac{r_{CeO_2,\lambda}}{r_{ref,\lambda}} \tag{5}$$

where L_{CeO_2} and L_{ref} are the detector signals for the ceria and reference samples, respectively. The spectral hemispherical reflectivity of the reference sample, $r_{ref,\lambda}$, is given by the manufacturer in the range of $250 \le \lambda \le 2800$ nm (Labsphere AS-01161-060, SphereOptics Zenith Polymer Diffuse Reflectance Standard – 50%).

2.2. Photodetectors

Three types of photodetectors were used to cover the wide range of wavelengths of interest: a SiC photodiode, a InGaAs photodiode and a PbS photoconductor covered the ranges 250–1000 nm, 800–1700 nm and 1000–2800 nm, respectively, and 20, 50 and 100 consecutive measurements were performed at each wavelength (50 nm steps), respectively. An increasing number of consecutive measurements was performed at longer λ to minimize the measurement error based on background noise because, for $\lambda > 1200$ nm, the Xe-arc has a decreasing emission with wavelength leading to weak detector signals. The accuracy of the measurement was 95%, determined with the reference sample.

2.3. Ceria samples

Disk-shaped ceria pellets (23 mm-dia., 4 mm-height) were manufactured by pouring a slurry of Cerium (IV)-oxide (99.9%

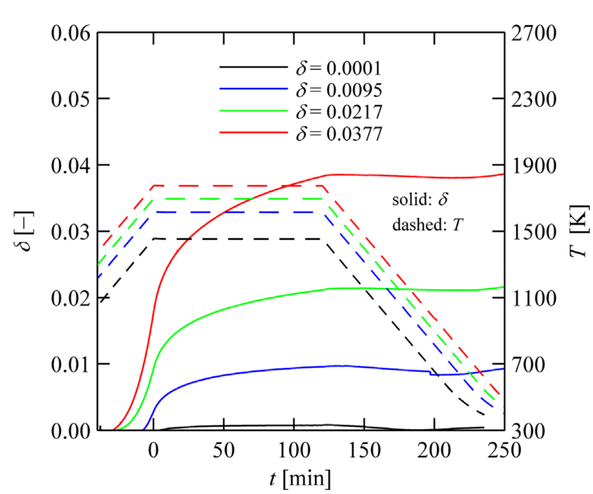

Fig. 2. Nonstoichiometry (solid) and temperature (dashed) of ceria as a function of time during a TGA run.